Journal of Catalysis 257 (2008) 71–80

Contents lists available at ScienceDirect

Journal of Catalysis

www.elsevier.com/locate/jcat

Support effects in HDS catalysts: DFT analysis of thiolysis and hydrolysis energies of metal–support linkages

Yogesh V. Joshi [a], Prasenjeet Ghosh [b], Michel Daage [b], W. Nicholas Delgass [a,*]

[a] Purdue University, West Lafayette, IN 47907, USA
[b] ExxonMobil Research and Engineering Company Annandale, NJ 08801, USA

ARTICLE INFO

Article history:
Received 26 November 2007
Revised 3 April 2008
Accepted 11 April 2008

Keywords:
HDS
Molybdenum support interactions
HDS Type-I versus Type-II behavior
Catalyst descriptors
Thiolysis
Sulfidation
DFT

ABSTRACT

We have carried out a theoretical investigation of the active phase–support interaction for HDS catalysts using density functional theory to calculate the thiolysis and hydrolysis reaction energies for the metal–support linkages. These metal–support linkages are represented by simplified cluster models with –SH or –OH terminations to represent the sulfide (active) and oxide (support) phases, respectively. The calculated rank order of the supports representing Type-I (strong interaction) tendency (SiO_2 < carbon < Al_2O_3 < TiO_2 < ZrO_2 < Y_2O_3) is in agreement with the experimentally observed behavior. Based on the calculated energetics the temperature-induced Type-II nature of the MoS_2–Al_2O_3 interaction is predicted by a higher equilibrium constant of the thiolysis reaction at higher temperature. Thus, the thiolysis energy provides a qualitative scale of the Type-I/Type-II nature of the support and is, therefore, a useful descriptor of catalytic behavior.

1. Introduction

In order to meet the future regulations for allowed sulfur content in gasoline and diesel fuels, an order of magnitude improvement in the efficiency of the hydrodesulfurization (HDS) processes is desired. Reaching that goal will include optimization of process conditions as well as discovery of new HDS catalysts. HDS catalysts are typically mixed metal sulfide materials impregnated on some amphoteric or acidic oxide support. The nature of support used in the catalyst plays a significant role in determining its activity as reviewed recently by Dhar et al. [1]. In addition to alumina (Al_2O_3), various other metal-oxides such as SiO_2, TiO_2 [2,3], ZrO_2 [4,5] and MgO [6] have been experimentally investigated. Novel catalytic supports such as zeolites [7], mesoporous materials [8–10] and clays [11] have also been proposed in the literature. It was found [2,3] that supports such as TiO_2 and ZrO_2 lead to catalysts with higher intrinsic activity. The choice of the support has important implications for catalyst properties, such as aging and deactivation, regeneration, reducibility, and ease of sulfidation, as well as the recovery of the spent catalysts. For example, use of carbon as the support provides a strategic advantage in terms of the recovery of the precious metal. However, the limited surface area and weak mechanical properties have prevented the commercialization of many of these supports.

In order to overcome the shortcomings of the individual single metal-oxide systems, binary mixtures of these have been recently pursued in the literature. The TiO_2–Al_2O_3 system, taking advantage of the higher activity of the titania and higher surface area of the alumina, is the important one with considerable scientific and commercial presence [12–16]. Such supports are prepared by co-precipitation, impregnation, chemical vapor deposition and grafting [13,17]. Other combinations of the mixed metal-oxide supports, such as SiO_2–Al_2O_3, B_2O_3–Al_2O_3, and ZrO_2–Al_2O_3, have also been tried and reviewed recently by Dhar et al. [1]. The dispersion, acidity (both Brønsted and Lewis), and redox properties of the support are highly dependent on the preparation method of the mixed metal oxides.

In this paper, we study the effect of different metal-oxides as supports for HDS catalysts using theoretical methods. We have focused on the supports for two primary reasons: (1) changing support properties is the easiest and most economic way to manipulate microscopic properties for commercial scale synthesis of the catalyst and (2) active phase–support interactions are not completely understood for HDS catalysts. In particular, our emphasis is on the interaction of transition metal sulfides (active phase) with the oxide supports and quantifying the nature of such interactions.

1.1. Type-I and Type-II supports

Metal–support interactions have long been known to play an important role in HDS catalysts. FTIR has shown [18–21] that

* Corresponding author.
E-mail address: delgass@ecn.purdue.edu (W.N. Delgass).

0021-9517/$ – see front matter
doi:10.1016/j.jcat.2008.04.011

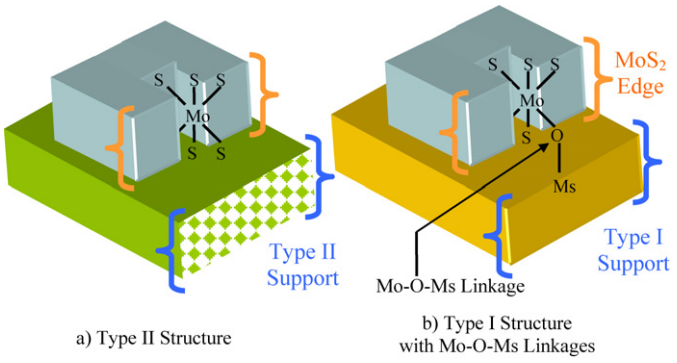

Fig. 1. Schematic representation of the (a) Type-II and (b) Type-I structures showing the metal sulfide and support interaction.

oxide-supports tend to form chemical linkages with the Mo atoms of the MoS_2 phase. After deposition of the active metals from solutions, these catalysts are calcined at 400 to 600 °C when most of the metal–support linkages are formed. The tendency for the formation of such linkages differs from one support to another and it is also dependant on the sulfidation conditions. The catalysts with higher tendency of formation of such linkages are known as "Type-I catalysts." The absence of such linkages leads to "Type-II catalysts." Effect of such linkages on the morphology of the MoS_2 particles has been observed directly by Hensen et al. [22]. It is well established that use of alumina (Al_2O_3) as a support leads to the smaller MoS_2 particles since the metal–support interaction (i.e. chemical linkage between MoS_2 and Al_2O_3, see Fig. 1) inhibits the free lateral growth of the MoS_2 crystallite. Such inhibition is in-fact advantageous as it leads to smaller crystallites and consequently higher dispersion [22]. Further, as a consequence of these interactions, the mobility of the MoS_2 particles on the support surface is hindered, thereby preventing the sintering during calcination or sulfidation treatment. DFT investigation by Hinnemann et al. [23] has shown the spatial and quantitative nature of such metal–support interaction. These authors report that MoS_2 tends to form linkages to the support through oxygen atoms only on the periphery (edge) of the MoS_2 basal planes. Formation of such linkages from the bulk atoms (non-peripheral) atoms is energetically not favorable.

In addition to its formation of chemical linkages, the support also has an electronic effect on the transition metal–sulfide crystallite. DFT results by Hinnemann et al. [23] show that the molybdenum–sulfur binding energy at the MoS_2 edge increases upon formation of Mo–O linkages to the support. This was rationalized based on the increased polarity of the Mo–S bond in the vicinity of the Mo–O linkages. It was further observed that H_2 binding energy to such S atoms goes down with increasing S binding energy. Since S vacancies are considered as active HDS sites, the intrinsic activity of Type-I structures is expected to be lower. Questions that remain about these linkages are: (a) Why do some supports give rise to Type-I structures while others do not? and (b) Why does the formation of the Type-I or Type-II structures depend on the synthesis conditions?

The binding orientation of the MoS_2 particles has been studied extensively using transmission electron microscopy (TEM) and is important for determining the total MoS_2 edge area available for HDS reactions. MoS_2 particles are [24] bonded by basal planes on the (111) surface of Al_2O_3, while on the (100) surface, edge bonded particles dominate. On TiO_2 surfaces, the epitaxial similarity between the (110) surface of MoS_2 and the (001) surface of TiO_2 leads to formation of the edge bonded MoS_2 particles. It has also been shown that the concentration and the nature of the surface hydroxyl groups is sensitive to the epitaxial arrangement and surrounding conditions (p_{H_2O}, p_{H_2}, and T). For example, using ab initio calculations, Toulhoat and coworkers [25] found that a γ-Al_2O_3 (110) surface is highly hydroxylated as opposed to a (100) surface, which shows only Lewis acidity at temperatures above 600 K. Other model support studies include work by de Jong et al. [26] focusing on MoS_2 on SiO_2/Si(100) epitaxial growth. Their investigation included XPS (X-ray Photoelectron Spectroscopy), AFM (Atomic Force Microscopy), RBS (Rutherford Backscattering) and SIMS (Secondary Ion Mass Spectrometry) to show the sulfidation mechanism of Mo oxides on SiO_2 films. According to this mechanism the sulfidation of MoO_3 to MoS_2 proceeds through Mo(IV) oxysulfide. Other model support studies include Ni–W–S and Co–W–S on SiO_2/Si(100) to study the effects of chelating agents by Kishan et al. [27,28]. For such model supports, differential charging of the catalyst (common for the regular support) is prevented during XPS measurements. Resulting narrow XPS lines are easier to interpret in terms of the change in the oxidation state of the active metals. It was shown [27] that addition of the chelating agents prolongs the sulfidation of the Ni-containing phase. It was proposed that the chelating agents, such as CyDTA, complex with the Ni. The decomposition of the chelating agent was found to be coincident with the sulfidation of the Ni phase. Similar study of the CoWS system indicated that use of the chelating agents promotes the synergy of the two sulfide phases. These results indirectly suggest that the chelating agents can selectively modify the metal–support interaction by complexing with one of the transition metals.

Recently there have been several excellent reviews of the current level of the experimental and theoretical understanding of hydrotreating catalysts. A review by Besenbacher et al. [29] has covered recent aspects of the combined STM and DFT understanding of the MoS_2 particle shape and its dependence on the catalyst composition. A couple of recent papers [30,31] by Raybaud and coworkers have focused on a predictive approach to improve the HDS catalysts. Using recent advances in theoretical understanding [30], the group has focused on the metal–sulfur bond energy as the base descriptor for fine tuning the catalyst performance and proposed an improved NiMoWS catalyst [31].

Arrouvel et al. [25,32,33] carried out very detailed investigations of Mo_6S_n ($n = 10$ to 24) cluster binding on γ-Al_2O_3 and anatase (TiO_2) using DFT. These authors [25] quantify two types of metal–support interactions for determining the orientation and stoichiometry of the MoS_2 particle on these supports. The "chemical ligand effect," which is equivalent to chemical bonding, dominates the binding of smaller MoS_2 particles on the supports. As MoS_2 particle gets larger the "physical ligand effect," which is equivalent to a physisorption interaction, tends to dominate over the chemical ligand effect due to the larger number of S atoms involved in the van der Waals interaction with the support. It is expected that with increasing particle size the chemical ligand effect which is equivalent to number of the chemical bonds between the active phase grows only with particle radius, r, while the physical ligand effect grows with r^2. Arrouvel et al. [25] confirm that the chemical ligand effect is mainly governed by the epitaxial relationship between the support and the MoS_2 phase. The physical ligand effect depends on the tendency of the support surface to remain hydroxylated for the given temperature and partial pressures (T, p_{H_2S}, p_{H_2} and p_{H_2O}). It was found [25] that for Al_2O_3, the physical ligand effect remains dominant for small MoS_2 particles (diameter > 10 Å) and the preferred binding mode is parallel to Al_2O_3 surfaces (110 and 100). Under this binding mode, the sulfur coverages (S/Mo ratio) are higher than the expected coverages for the isolated MoS_2 particles as higher S-coverage leads to better van der Waals stabilization. In case of the anatase, MoS_2 particles as large as 45 Å tend to be edge-bonded due to epitaxial compatibility. The higher S-vacancies associated with such particles have been proposed [25] as a reason for the higher activ-

ity. A recent report by Costa et al. [34] indicated that in addition to the higher vacancy formation, a higher Mo-edge/S-edge ratio induced by the epitaxial order of the anatase surface could be another reason for higher intrinsic activity of the MoS_2 supported on TiO_2 compared to alumina. A similar comparison was made for the promoted MoS_2 system. It was concluded that the edge wetting phenomena is important for determining the promotion effect and metal–support interaction.

Explanation of the catalyst–support interactions based on epitaxial relations is not universally applicable for real catalyst surfaces (especially with porosity and mixed oxides) which tend to lack extended epitaxial order. These supports may maintain an epitaxial order on a small scale, but direct evidence for its importance is lacking as the small catalyst particles are the hardest to see by electron-microscopic techniques. In such cases the opportunistic bonding between the support and active sulfide phase may be important. Under such conditions the number and strength of the metal–support linkages (Mo–O–$M_{(S)}$) would guide the differences among different supports. The number of Mo–O–$M_{(S)}$ bonds is related to the strength (energy of dissociation) of such linkages through a standard chemical equilibrium. However, there would be a limit on the maximum possible linkages set by the number of surface hydroxyl groups (–OH) available.

1.2. Objective of this work

Theoretical description of the metal–support interaction is a complex and challenging problem and, to our knowledge, even a simple scale for rank-ordering of different supports is lacking. Published literature merely recognizes the presence (Type-I) or absence (Type-II) of metal–support interactions. Such a classification of supports as either Type-I or Type-II is rather oversimplified, since the reality is that there is a continuum, as opposed to two broad categories, depending on the strength of the metal–support interactions. In this paper, we develop such a continuous scale to quantify the metal–support interaction. This scale is critical for two important reasons: First, it allows a rational procedure for choosing the optimum support for the catalyst depending on the metal–support interaction needed, and second, it allows a quantitative interpretation of the effect of support on the activity of a HDS catalyst. The utility of this scale is illustrated through the following example. It is known [35] that at low loading of the Mo on Al_2O_3, the Mo–Al_2O_3 interaction is so strong that sulfidation of such catalysts is rather difficult. Thus for a catalyst containing low Mo loading, a support with lower tendency to form Type-I structure is desirable. Using a scale such as that proposed in this paper, one can now identify the best support for such a catalyst. Conversely, strong interaction would be better for higher Mo loadings where sintering must also be controlled.

We would also like to correlate this scale to the electronic description of the metal–support linkages in order to identify atomic descriptors which govern (or explain) the Type-I or Type-II behavior of supports.

The rest of this paper is organized as follows. In Section 2, we discuss model reactions to characterize metal–support interactions. We also outline the details of the theoretical method in that section. Results and discussion are covered in Section 3, followed by a summary of the important conclusions in Section 4.

2. Details of calculations

2.1. Model for metal–support interactions

Modeling metal–support interactions at the atomistic level is a major challenge to computational chemists because of the complexity and the diversity of the possible model structures. A simplified atomistic picture of the material offers two-fold advantage: (a) The number of different possible structures is limited and the observed effects can be related to inherent properties of the atoms involved; (b) the problem is computationally tractable for a variety of the elements across the periodic table.

Table 1
Calculation details of various atomic species and their $M(OH)_N$ counterparts

Element symbol	Coordination number (N)	EN[a]	Basis set	Mulliken charge[b]	NBO charge[b]	M–O bond length (Å)
Si	4	1.90	6-31g(2df)	0.54	2.36	1.63
C	3 (sp^2)	2.55	6-31g(2df)	0.41	0.31	1.36
Al	3	1.61	6-31g(2df)	0.85	1.95	1.69
Ti	4	1.54	6-31g(2df)	1.20	1.89	1.81
Zr	4	1.33	lanl2dz	1.52	2.34	1.97
Y	3	1.22	lanl2dz	1.26	2.17	2.04
Mo	4	2.16	lanl2dz	1.35	1.64	1.90
W	4	2.36	lanl2dz	1.25	1.63	1.88
Co	3	1.88	6-31g(2df)	0.85	1.34	1.73
Ni	2	1.91	6-31g(2df)	0.65	0.99	1.69
O	2	3.44	6-31g(2df)	–	–	–
S	2	2.58	6-31g(2df)	–	–	–
H	1	2.20	6-31g(p)	–	–	–

[a] Pauling electronegativity.
[b] Charge on M in $M(OH)_N$.

It is well established that for commercial HDS catalysts (CoMoS etc.) the active catalytic phase is in the sulfide form. For such catalysts, the precursor species are often present in their oxide form. On sulfidation, the transition metal-oxide phase converts into the sulfide phase. As the experimental evidence suggests, there exist Mo–O–$M_{(S)}$ linkages between the support and the Mo phase. These linkages are developed [35] during the formation of the transition metal-oxide phase, and originate from the –OH groups [35] initially present on the support oxides. However, during sulfidation most of the well dispersed Mo oxide species reorganize to form MoS_2 particles. In that process, a majority of the –OH groups are regenerated. However, it has been speculated [35] that these –OH groups remain hydrogen bonded to sulfur atoms from MoS_2 particles. Thus, during the sulfiding process, Mo–O–$M_{(S)}$ bonds are broken and can play an important role in determining the operating state of the catalyst.

The Mo–O–$M_{(S)}$ linkages can affect both the activity and morphology of the active phase of the catalyst. In order to study these effects using DFT, several approximations have to be made to simplify the catalyst model. Hinnemann et al. [23] studied the electronic effect of the Mo–O– linkages by replacing the O–$M_{(S)}$ support-structures by –OH groups. Such an approximation is equivalent to replacing the support oxide (starting from support metal $M_{(S)}$) with a single hydrogen atom. Although this approximation gives the qualitative electronic effect of the Type-I structures, it cannot capture the effect of changing from one support to another. As the Pauling electronegativity of the support metal varies over a large range (1.22 for Y to 2.36 for W, as shown in Table 1), the polarity of the Mo–O–$M_{(S)}$ linkages is expected to vary from one support metal atom to other. For example, Pauling electronegativies of hydrogen (2.20) and aluminum (1.61) are significantly different and thus cast doubt on the ability of a hydrogen atom to approximate alumina.

It is known [18] that increasing sulfidation temperatures often leads to breaking of the Mo–O–$M_{(S)}$ linkages thereby increasing the Type-II character. Candia et al. [18] have previously estimated that $CoMoS/Al_2O_3$ Type-II catalysts formed by high temperature sulfidation at 873–1275 K were twice as active as Type-I formed by regular sulfidation at 675 K. This strongly suggests that the number of the Mo–O–$M_{(S)}$ linkages is the governing factor in determining the Type-I characteristic of the active phase. The total number of these linkages should be governed by the strength of these linkages. Therefore, we hypothesize that the strength of Mo–O–$M_{(S)}$

linkage is the driving factor for the Type-I or Type-II character of the support.

Hinnemann et al. [23] suggested that the strength of the Mo–O–$M_{(S)}$ linkage can be measured in terms of the energy required to break or form such a linkage. We propose therefore, that at least on a relative basis, that energy can be calculated as the reaction energy of the simple thiolysis reaction, written as:

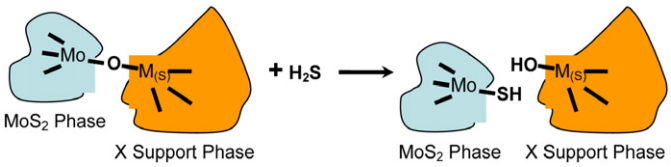

thiolysis:

$$(MoS_2\ \text{phase})\text{–O–(X support)} + H_2S \rightarrow (MoS_2\ \text{phase})\text{–SH} + \text{HO–X}\ldots, \quad (1)$$

where X represents the support in the form of metal-oxide such as Al_2O_3 or SiO_2 or TiO_2 and MoS_2 represents the bulk sulfide phase. Thus, (MoS_2)–O–X in reaction (1) is an approximate representation of the supported catalyst (e.g. MoS_2 on Al_2O_3) and the strength of the metal–support interaction is quantified with the reaction-energy of (1). Certainly, reaction (1) is not the only way to compute the strength of the metal–support interaction. Other possible ways include breaking such linkages in reactions (2) and (3). Reaction (2) is also thiolysis, but unlike in reaction (1), OH bonds are formed with MoS_2 as opposed to SH. In reaction (3), a hydrolysis takes place, instead of thiolysis. There is a distinct possibility of all these reactions occurring during the sulfidation process as both H_2O and H_2S are present in the sulfiding mixture. Hence, consideration of these possibilities allows us to compare the thermodynamic feasibility of these different reactions:

thiolysis:

$$(MoS_2)\text{–O–X} + H_2S \rightarrow (MoS_2)\text{–OH} + \text{HS–X}\ldots, \quad (2)$$

hydrolysis:

$$(MoS_2)\text{–O–X} + H_2O \rightarrow (MoS_2)\text{–OH} + \text{HO–X}\ldots. \quad (3)$$

Reactions (1)–(3) capture the strength of these linkages when the catalyst is already in the sulfided form. However, many of these linkages are formed during the actual synthesis of the catalyst when the Mo is in the oxide form [36]. Therefore the formation of Mo–O–$M_{(S)}$ linkages can be studied by the reaction energy of the following condensation reaction, where the Mo is in the oxide form:

condensation:

$$(MoO_3)\text{–OH} + \text{HO–X} \rightarrow (MoO_3)\text{–O–X} + H_2O\ldots. \quad (4)$$

The energy released during the formation of the Mo–O–$M_{(S)}$ bond can also be taken as the strength of the Mo–O bond. Finally, we note that the hydrolysis reaction (3) is the reverse of the condensation reaction (4), except for the form of the bulk molybdenum phase. For hydrolysis, the bulk Mo-phase is a sulfide while for condensation the bulk Mo phase is represented by the oxide.

Up to this point, the discussion has concerned the linkages between two solid phases, namely, the support and the active sulfide catalyst. The simplest model for calculating the strength of such a linkage would be the gas phase thiolysis reaction (5). This reaction is a generalized thiolysis reaction for an oxygen linkage between active metal ($M_{(A)}$) and support metal ($M_{(S)}$). The sulfided form of the transition-metal is approximated by terminating the transition metal ($M_{(A)}$) with –SH bonds (maintaining the proper coordination) and the oxide support is approximated by adding –OH groups to the support metal atom ($M_{(S)}$). Reactions (5) and (6) are equivalent in the sense that they represent the two different possibilities for product formation depending on how the split OH (from the metal–support interaction) and SH (from H_2S) reattach themselves in the product:

thiolysis:

$$(SH)_nM_{(A)}\text{–O–}M_{(S)}(OH)_m + H_2S \rightarrow (SH)_nM_{(A)}\text{–SH} + \text{HO–}M_{(S)}(OH)_m\ldots, \quad (5)$$

thiolysis:

$$(SH)_nM_{(A)}\text{–O–}M_{(S)}(OH)_m + H_2S \rightarrow (SH)_nM_{(A)}\text{–OH} + \text{HS–}M_{(S)}(OH)_m\ldots. \quad (6)$$

The coordination numbers for $M_{(A)}$ and $M_{(S)}$ ($n+1$ and $m+1$, respectively) are chosen according to the most commonly observed oxidation states for different metal species. These oxidation-state based coordination numbers are listed in Table 1, which includes the metal species commonly used in HDS catalysis either as a support or as the active sulfide phase. In the bulk oxide phase of the support the actual coordination may be higher. For example in TiO_2 (rutile), Ti is octahedral with coordination number of 6. However, the coordination number for the –OH groups is selected according to the oxidation number which is based on the charge neutrality of the bulk phase. For TiO_2 the number is 4. In general we have kept a maximum coordination number of less than or equal to 4. A higher coordination number of 6 leads to multiple bridge bonding of –OH groups because the constraints on the oxygen imposed by the bulk structure were absent at this level of cluster approximation. In order to keep the coordination number from exceeding 4, we have taken MoO_2 as the reference oxide phase for molybdenum instead of the more stable MoO_3 phase. While the MoO_2 phase is not the most stable phase for oxide form of the molybdenum, the coordination number of 4 well-represents the +4 Mo oxidation state of the bulk MoS_2 phase. The schematic representation of the thiolysis of Mo–O–Si and Mo–O–Al linkages is shown in Figs. 2a and 2b, respectively.

To model the interaction with a carbon support, a different approximation of the support has to be introduced. We assumed that Mo–O–C linkages would be formed on the edges of a graphene sheet, which we represented by a single phenyl (benzene ring) group attached to Mo through bridging oxygen. Such thiolysis is schematically depicted in Fig. 2c.

In order to draw a correlation between the DFT calculated reaction energies and easily available elemental properties of the metals, we tabulated various structural and electronic parameters against the electronegativity (Pauling's scale) of the elements. Such correlations are extremely important for understanding the observed behavior. An example will be discussed in a later section.

2.2. Theory details

For all of our calculations, we used a Becke three-parameter hybrid exchange functional [37], along with a Lee, Yang, and Parr correlation functional [38] (B3LYP). For all the light elements (O, S, Si, Al, Ti, Co and Ni), we used a double zeta basis set with two polarization [39] functions: 6-31g(2df). For heavy elements such as Y, Zr, Mo and W, we used a pseudopotential basis set LANL2DZ [40–42]. This represents a valence double zeta basis set with core electrons replaced by the relativistic pseudopotential. All of our calculations were done using the Gaussian 03 software package [43]. The reported energies include contributions from zero point energies. We have also recalculated all the reaction energies with a triple-zeta basis set for the light atoms. We find that the calculated reaction energies are linearly correlated to the reaction energies calculated using double-zeta basis. Thus, we believe that although absolute reaction energies are not converged, the differences between reaction energies are. This allows us to compare the thiolysis energies corresponding to different supports even without absolute convergence. The electronic analysis of the calculated density was carried

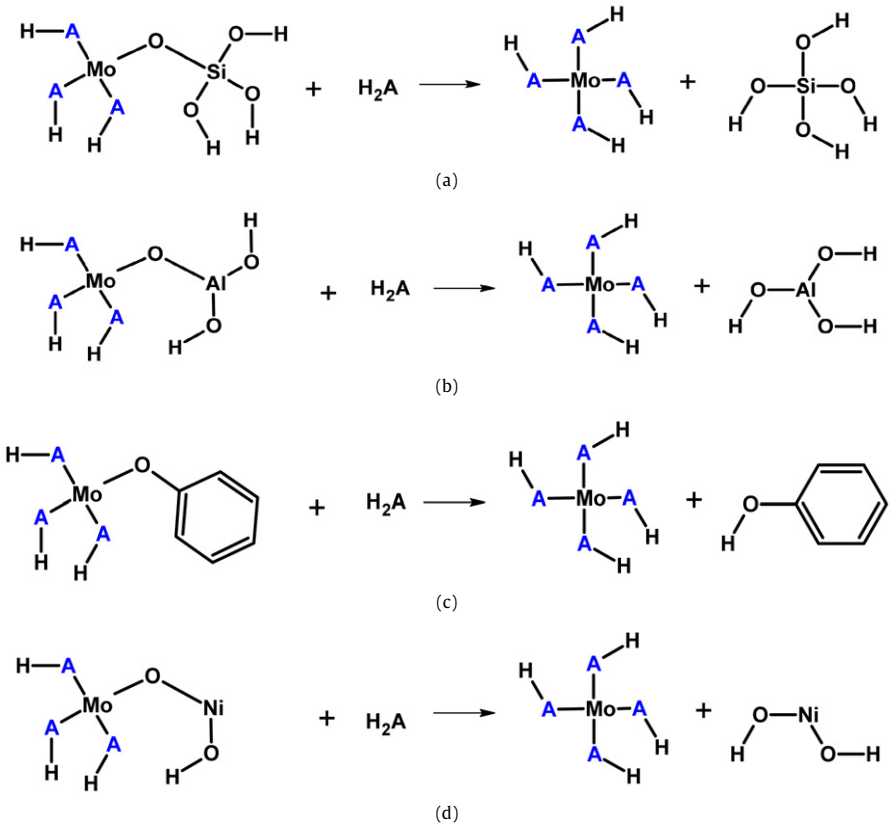

Fig. 2. Generalized thiolysis reaction (A = sulfur) or hydrolysis reaction (A = oxygen) for different coordination situations of the support: (a) tetrahedral Si(IV); (b) trigonal Al(III); (c) phenyl carbon; (d) Ni(II).

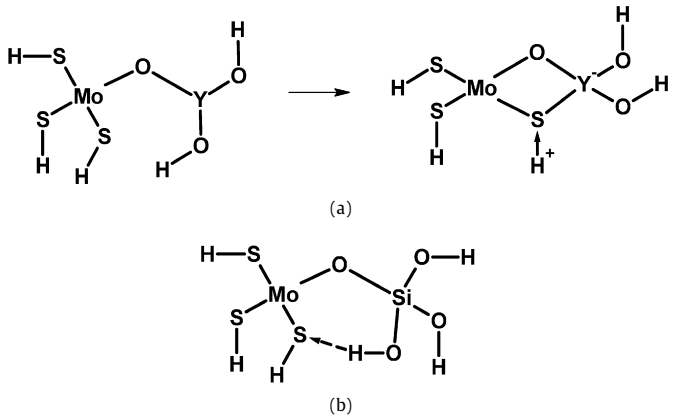

Fig. 3. (a) Lewis acid–Brønsted acid site transformation by geometrical rearrangement; (b) hydrogen bonding between –SH and –OH groups.

out using the Natural Bonding Orbital (NBO) method proposed by Weinhold et al. [44–46]. In NBO analysis, the electronic density is projected onto the natural atomic orbitals (NAO) which are similar to spherical harmonics centered on each atom. The NBOs are constructed using the linear combinations of the NAOs. Since NBO charges have better convergence with the increasing the basis set [46], NBO charges are not checked against higher basis sets.

In order to measure the strength of the Mo–O–$M_{(S)}$ linkage, it is essential to maintain the single bridging species covalently bonded between two metal atoms. Any additional bonding interaction between the two metal species will lead to incorrect characterization of the bond strength proposed in terms of thiolysis reaction (5). In some cases, the hydroxyl or thiol groups tend to coordinate with both metal species as the distance between the two decreases during geometry optimization. This situation is more frequent for Al and Y, where the tri-coordinated metal species have inherent Lewis acidity. Such metals have a tendency to coordinate with an additional –OH or –SH group to generate Brønsted acidity as shown in Fig. 3a.

Geometries of such linked clusters, although energetically more stable, do not represent a single $M_{(A)}$–O–$M_{(S)}$ linkage between two metal species. Such rearrangements are the consequence of the finite structure of the models used to represent the $M_{(A)}$–O–$M_{(S)}$ linkage. Naturally, the thiolysis or hydrolysis energy of such a compound is higher (more endothermic) than the expected energy for thiolysis of a single linkage. To avoid formation of these species, the $M_{(A)}$–O–$M_{(S)}$ angle was constrained to a certain value. In some cases the constraint was added only initially to guide the structure to local minima. Once such a minimum was reached, the constraint was removed and structure was reoptimized. The only two struc-

Table 2
Calculated geometries and energy parameters for thiolysis of Mo–O–$M_{(S)}$ linkages

	ΔE[a] (kcal/mol)	ΔE[b] (kcal/mol)	Mo MC[c]	Mo NBOC[d]	Mo–O length[e] (Å)	Mo (%)[f]	Mo d (%)[g]	$M_{(S)}$ MC[c]	$M_{(S)}$ NBOC[d]	O–$M_{(S)}$ length (Å)[e]	$M_{(S)}$ (%)[f]
Si	−3.2	54.3	1.17	0.60	1.92	13.3	91.4	0.32	2.43	1.63	14.1
$-C_6H_5$	0.4	43.2	1.06	0.64	1.88	14.8	78.2	0.30	0.26	1.36	30.9
Al	1.8	50.8	1.14	0.69	1.85	17.7	90.0	0.83	2.03	1.71	8.9
Ti	3.6	53.0	1.15	0.55	1.92	15.3	78.5	1.30	1.90	1.79	10.4
Zr	10.6	60.1	1.12	0.69	1.83	18.4	83.5	1.56	2.29	2.06	6.9
Y	13.9	69.3	1.12	0.70	1.81	20.4	86.2	1.37	2.21	2.14	1.9
Mo	23.4	56.6	0.96	0.41	1.94	22.4	92.7	1.53	1.71	1.87	27.3
W	23.9	76.5	0.90	0.33	2.00	21.9	94.6	1.68	2.06	1.84	21.6
Co	7.6	39.6	1.06	0.60	1.85	21.1	84.1	0.78	1.27	1.85	22.2
Ni	12.7	44.0	1.15	1.15	1.83	23.2	91.7	0.70	1.04	1.72	20.3

[a] Thiolysis energy for breaking Mo–O bond.
[b] Thiolysis energy for breaking O–$M_{(S)}$ bond.
[c] Mulliken charge.
[d] NBO (Natural Bond Orbital) charge.
[e] Bond length in Å.
[f] Contribution of Mo NBO to Mo–O bond.
[g] Fraction of d orbital in Mo NBO.

tures involving thiolysis for which we could not locate the local minimum were Mo–O–Y and Mo–O–Ni. We have carried an out potential energy scan for the Mo–O–$M_{(S)}$ angle for these structures. Based on those calculations, we can ascertain that the effect of the angle constraint is much smaller (less than 0.5 kcal/mol) than the actual thiolysis energy. The simplification is not a concern since in reality the –OH and –SH groups would not be present in the extended structure of the support and active metal–sulfide phase. There is a distinct possibility of hydrogen bond formation between the –OH and –SH groups belonging to two different metal species. In Fig. 3b, we have schematically shown an example of hydrogen bonding for the $Mo(SH)_3$–O–$Si(OH)_3$ species. Such hydrogen bond formation often leads to a slightly different geometry due to the added energy constraint. The energetic effect of hydrogen bond formation is expected to be minimal, however, compared to reaction energy for thiolysis or hydrolysis.

3. Results and discussion

3.1. Thiolysis reaction

In Fig. 2, we have shown the thiolysis reaction scheme (A = sulfur) for some representative supports, based on the general scheme proposed earlier in reaction (5). The reaction produces two products: (a) hydroxyl terminated support atoms and (b) molybdenum thiol. The reaction scheme shown in (5) or Fig. 2 assumes that the Mo–O bond is the more labile bond compared to the O–$M_{(S)}$ bond (i.e. the bond between the oxygen and support metal atom) and breaks under sulfiding conditions. However, one could also argue that thiolysis can break the O–$M_{(S)}$ bond as well. In Table 2, we have listed energetics and important electronic and geometry parameters of different Mo–O–$M_{(S)}$ linkages. Comparison of the reaction energies (initial two columns of Table 2) indicates that the Mo–O bond is much weaker compared to the O–$M_{(S)}$ bond, regardless of what the support metal (M_S) is, including the case where support metal atom is represented by Mo. This special case, $Mo(SH)_3$–O–$Mo(OH)_3$ is illustrative as it highlights the differences in the nature of the two molybdenum atoms depending on their attached ligands. If we look at the % contribution to Mo–O bonds by each of the Mo atoms, the $Mo(SH)_3$–O bond (% Mo contribution = 22.4%) is equally covalent compared to the O–$Mo(OH)_3$ bond (% Mo contribution = 27.3%). Hence the difference in the thiolysis energies of these Mo–O bonds is not due to differences in covalency. The higher positive charge on the $Mo(OH)_3$ (support metal atom Natural Bond Orbital Charge: NBOC of 1.71) compared to the sulfided Mo in $Mo(SH)_3$ (NBOC of 0.41) indicates that although the O–$Mo(OH)_3$ bond is equally covalent, the additional 3 –OH groups on the Mo support metal atom makes charge separation more substantial. Such induced polarity along with similar covalency makes the O–$Mo(OH)_3$ bond stronger compared to the O–$Mo(SH)_3$ bond. The two thiolysis reactions (5) and (6) give rise to completely different products. The difference in the reaction energies can also be attributed to the difference in product stability. The support atom (Mo for the current discussion) bonded to –OH groups is more cationic compared to Mo bonded to –SH groups. This seems to indicate that the –SH group tends to bond to the less cationic Mo atom and vice versa for the –OH group. In the opposite scenario, the stability of the products is expected to be lower due to the mismatch between the bond polarities and natural covalency of the Mo–O, Mo–S bonds. Thus, the combined energy of the $Mo(OH)_4$ and $Mo(SH)_4$ species will be much lower than that of $Mo(OH)_3(SH)$ and $Mo(OH)(SH)_3$. This also conforms to the absence of the thiol groups on the catalyst supports as they are likely to be replaced by more stable –OH groups.

3.2. Thiolysis reaction energy and Type-I/Type-II nature of the support

From Table 2, it is clear that the Mo–O bond in Mo–O–$M_{(S)}$ is the weakest for $M_{(S)}$ equal to Si, while bond strength increases in the order Si < C < Al < Ti < Zr < Y. This trend, therefore, represents a prediction of the extent of Type-II and Type-I structures on the support. For instance, the weak Mo–O bond in silica and carbon makes them Type-II supports, whereas the stronger Mo–O bond on alumina, titania or zirconia makes them Type-I supports. Experimental literature [1,12,47] is also consistent with this observation for these supports.

Type-II structures are more active (on a per atom basis) than Type-I structures, however, they provide this higher activity at the cost of lower metals dispersion. Evidence from the literature [1] confirms that MoS_2 dispersion is lowest in silica and increases as C < Al < Ti. The implication of this result is that now we have a quantitative metric (based on thiolysis reaction energy) to rank different supports in order of the metals dispersion that can be achieved on them. This is significant as it provides a rational criterion to choose a support for the catalyst.

Although we established a “relative quantitative” scale for different supports, the absolute values of thiolysis reaction energies have certain quantitative importance as well. We find thiolysis of Mo–O–Si exothermic indicating that the equilibrium will favor dissociation of these linkages in the presence of H_2S. Similarly, for carbon such dissociation is almost thermo-neutral. This

Table 3
Thermochemical analysis of thiolysis equilibrium constants

	ΔH^a	ΔS^b	$e^{-\Delta G/RT}$						
			300 K	400 K	500 K	600 K	700 K	800 K	900 K
Silica	−3.6	5.6	7633.90	1660.72	665.00	361.28	233.65	168.51	130.68
Carbon	−0.5	−0.1	2.18	1.77	1.57	1.44	1.36	1.30	1.26
Alumina	1.0	−4.0	0.02	0.04	0.05	0.06	0.06	0.07	0.08

[a] Enthalpy of thiolysis at STP in kcal/mol.
[b] Entropy of thiolysis at STP in cal/mol-K.

clearly suggests the Type-II nature of both these supports. For Al the thiolysis reaction is endothermic by 1.8 kcal/mol. The relatively low endothermicity of the reaction indicates that equilibrium will favor thiolysis at higher temperatures. This potentially explains the formation of Type-II structures on Al_2O_3 after sulfidation is carried out at higher temperatures [18]. In order to see the quantitative behavior, we calculated the free energy change for thiolysis of the Mo–O–$M_{(S)}$ for silica, carbon and alumina. The thermochemical analysis of the optimized structures was done using frequency calculations under harmonic approximation. Internal rotational degrees of freedom were approximated by corresponding harmonic vibrations. To evaluate the effect of temperature on the equilibrium constant, we have neglected the effect of temperature change on ΔH and ΔS. Thus, ΔG is calculated as $\Delta H - T\Delta S$ for the entire temperature range reported in Table 3. It can be clearly seen in Table 3 that at high temperatures the equilibrium favors breaking of Mo–O–Al linkages. At higher temperatures, behavior of silica should remain largely Type-II. Since the free energy change for carbon support is close to zero, the thiolysis equilibrium constant is temperature independent with Type-II tendency. However, such use of thiolysis energies to predict the equilibrium quantitatively is difficult to justify considering the approximations involved in the model and the theory.

Highly endothermic thiolysis reaction for Zr and Y indicates that Mo will be highly dispersed on these surfaces. Recent results by Soled et al. [48] have confirmed the higher dispersion of CoMoS phase on a Y_2O_3/SiO_2 support. The higher dispersion was in concert with the observed smaller stack height and lateral width of the MoS_2 particles. The thiolysis energies for these supports are of the same order of magnitude as the thiolysis energy of the Mo–O–Mo linkages. This indicates that these supports will give rise to a highly dispersed molybdenum phase. Unless Mo loading (in terms of number of Mo atoms per unit area) is high, the absence of MoS_2 layers could be a distinct possibility. Highly endothermic thiolysis of the Mo–O–Mo is difficult to justify as the observation is that oxide phase of molybdenum can be easily sulfided. There are two possible reasons for this contradiction: (1) Thiolysis may not represent the reaction mechanism for sulfidation if molecular hydrogen along with H_2S plays important role; (2) The lower coordination number of Mo (4 according to MoO_2 phase) assumed in the model could be a source of the higher energies. A coordination number of 6 according to MoO_3 phase would lead to decrease in Mo–O bond strength and hence decrease the thiolysis energy.

3.3. Thiolysis energy and electronic structure correlations

Since the thiolysis reaction energy presents an important metric for discriminating different supports, it is of interest to investigate whether this energy depends on the electronic properties of the Mo–O–$M_{(S)}$ linkages. At the molecular level, the thiolysis reaction energy represents the bond breaking (Mo–O and H–SH bonds) and bond formation (O–H and Mo–SH bonds) energies. Natural Bond Orbital (NBO) analysis of the Mo–O and O–$M_{(S)}$ bonds may, therefore, be utilized to study the electronic properties of these bonds in more detail. In Table 2, we have listed some of the important

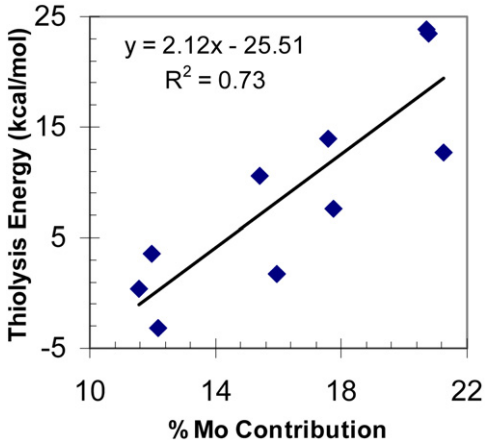

Fig. 4. Linear correlation between % contribution of Mo to the Mo–O NBO.

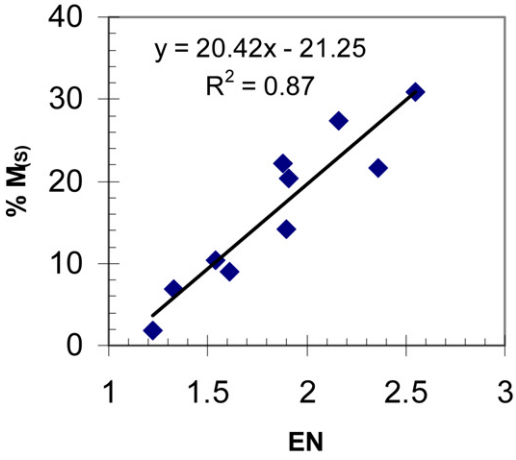

Fig. 5. Linear correlation between electronegativity (EN) and % metal contribution to the $M_{(S)}$–O bond.

electronic parameters calculated from the NBO approach. Of several different parameters investigated in this study, the percent (%) contribution of the Mo to Mo–O NBO most strongly correlated to thiolysis energy (correlation coefficient = 0.73). The Mo–O NBO is represented by the sigma overlap between Mo d-orbital and oxygen sp^3 hybrid orbital. The linear plot of thiolysis energy against the % Mo contribution to Mo–O NBO is shown in Fig. 4. Increasing Mo contribution to the Mo–O bond indicates increasing covalency of this bond. With increasing covalent nature, the bond becomes stronger leading to higher thiolysis energies.

3.4. Electronegativity scale and NBO analysis

We also find the expected linear correlation between the fraction of the electrons contributed by the metal to $M_{(S)}$–O NBO and the electronegativity (EN) of the metal $M_{(S)}$. EN of the oxygen atom on Pauling's scale is 3.44. With increasing EN of the metal, the polarity of the $M_{(S)}$–O bond should go down as the difference between the EN of O and $M_{(S)}$ goes down. Increasing electron occupancy in the NBO of the metal species provides direct evidence for the increasing covalent nature of the metal–oxygen bond with increasing electronegativity. As a consequence, we observe a linear correlation (as shown in Fig. 5) between EN and electron charge density on either the metal or the oxygen atom.

Table 4
Calculated geometries and energy parameters for hydrolysis of Mo–O–$M_{(S)}$ linkages

	ΔE (kcal/mol)[a]	Mo MC[b]	Mo NBOC[c]	Mo–O length (Å)[d]	Mo (%)[e]	Mo d (%)[f]	$M_{(S)}$ MC[b]	$M_{(S)}$ NBOC[c]	O–$M_{(S)}$ length (Å)[d]	$M_{(S)}$ (%)[e]
Si	−4.3	1.34	1.59	1.88	12.7	74.2	0.32	2.44	1.71	14.2
$-C_6H_5$	−0.9	1.39	1.68	1.94	14.4	75.3	0.31	0.32	1.36	32.7
Al	−2.1	1.35	1.56	1.88	12.8	74.5	0.74	2.02	1.71	9.1
Ti	0.8	1.35	1.55	1.86	20.3	81.1	1.31	1.89	1.87	14.9
Zr	6.8	1.33	1.53	1.86	20.6	84.3	1.56	2.30	2.05	9.3
Y	7.6	1.31	1.58	1.84	18.2	80.7	1.34	2.17	2.11	2.0
Mo	13.1	1.35	1.59	1.85	13.6	62.0	1.51	1.74	1.83	14.3
W	10.7	1.40	1.60	1.86	14.9	71.2	1.36	1.59	1.94	12.5
Co	7.2	1.46	1.69	1.81	16.5	97.9	0.91	1.36	1.77	18.2
Ni	28.7	1.56	1.60	1.78	22.6	87.8	0.37	0.86	1.71	15.6

[a] Hydrolysis energy for breaking Mo–O bond. For condensation change the sign of the energetics.
[b] Mulliken charge.
[c] NBO (Natural Bond Orbital) charge.
[d] Bond length in Å.
[e] Contribution of Mo NBO to Mo–O bond.
[f] Fraction of d orbital in Mo NBO.

3.5. Hydrolysis reaction energies

The thiolysis reaction energy explains breaking of the Mo–O–$M_{(S)}$ linkages during sulfidation. However, as described previously many of these linkages are formed during the calcination step of the catalyst synthesis, where the transition metals are in their oxide form. Condensation reactions (i.e. reverse of hydrolysis) would correspond to the formation of the Mo–O–$M_{(S)}$ linkages during calcination treatment. In order to study hydrolysis, we considered the full hydroxyl form of both active metal and support metal species [$M_{(A)}(OH)_n$–O–$M_{(S)}(OH)_m$] as the reactant, and the reaction can be represented by:

hydrolysis:

$$(OH)_nM_{(A)}\text{–O–}M_{(S)}(OH)_m + H_2O \rightarrow (OH)_nM_{(A)}\text{–OH} + HO\text{–}M_{(S)}(OH)_m\ldots. \quad (7)$$

The schematics of different hydrolysis reaction scenarios are shown in Fig. 2 (A = oxygen). In Table 4, we report the geometric and energetic parameters for the hydrolysis reactions. We found, as shown in Fig. 6, that the hydrolysis reaction is closely similar to the thiolysis reaction. With the exception of Ni, with a thiolysis energy of 12.7 kcal/mol but a hydrolysis energy of 28.7 kcal/mol, we find that the two reaction energies are linearly correlated. The condensation reaction (i.e. reverse of hydrolysis) energy for Mo with Si is more endothermic (4.3 kcal/mol from Table 4) than the exothermicity (−3.2 kcal/mol from Table 2) of thiolysis. This indicates that for silica the presence of Mo–O–Si linkages will be highly unlikely in the completely sulfided catalyst. For Al, both condensation (2.1 kcal/mol endothermic from Table 4) and thiolysis (1.8 kcal/mol endothermic from Table 2) have comparable reaction energies. For linkages between two Mo atoms, both thiolysis and hydrolysis are highly endothermic, indicating that the formation of the bulk phases is energetically more favorable compared to the formation of the Mo–O–$M_{(S)}$ linkages with regular supports, such as SiO_2 and Al_2O_3. This suggests that for supports like SiO_2 and Al_2O_3, the dispersed MoS_2 phase is in a metastable state. Thus in order to keep the Mo-oxide domains separate and to prevent sintering, regular synthesis procedures require use of dispersion aids (or chelating agents) such as nitrilotriacetic acid (NTA), ethylene diamine, ethylene diamine tetraacetic acid (EDTA), 1,2-cyclohexane diamine tetraacetic acid (CyDTA) [49,50]. Prins and coworkers [49,51,52] have shown that by adding these chelating agents the dispersion of the active phase is increased. At the same time low temperature sulfidation of Ni phase is prevented for better promotion of the MoS_2 phase.

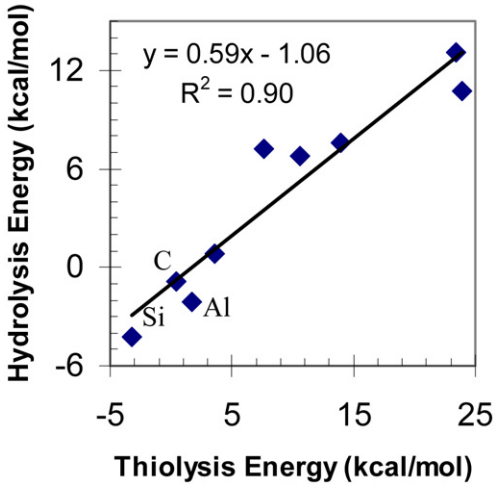

Fig. 6. Linear correlation between thiolysis energy and hydrolysis energy of metal support linkages.

3.6. Similarities between molybdenum and tungsten

Hydrodesulfurization catalysts based on molybdenum and tungsten sulfides are very similar in terms of their HDS activity [53] and form the bulk of the commercial catalyst portfolio today. We examined the differences between these two materials based on the thiolysis and hydrolysis reaction energy calculations for various W species. From Fig. 7, it is clear that tungsten forms stronger W–O–$M_{(S)}$ linkages compared to molybdenum. If we compare the thiolysis energy of the $Mo(SH)_3$–O–$Mo(OH)_3$ (23.4 kcal/mol) linkage to that of the $W(SH)_3$–O–$W(OH)_3$ (28.5 kcal/mol) linkage, it is expected that the cohesive energies of the bulk tungsten compounds should be higher compared to those of molybdenum. Both theoretical and experimental results regarding the cohesive energies (MoS_2 358 kcal/mol and WS_2 400 kcal/mol) of the two sulfides [54] confirm this observation. All these observations make us conclude that W has a larger tendency to form Type-I structures compared to Mo. There is a strong experimental evidence confirming this conclusion as it has been found [55,56] that MoO_3/Al_2O_3 is more reducible than WO_3/Al_2O_3. The difference in the behavior of the MoO_3 and WO_3 was attributed to the difference in the W–O and the Mo–O bond strength. It was [56] also noted that the difference in the bond strength arises from the differences in the bond polarities.

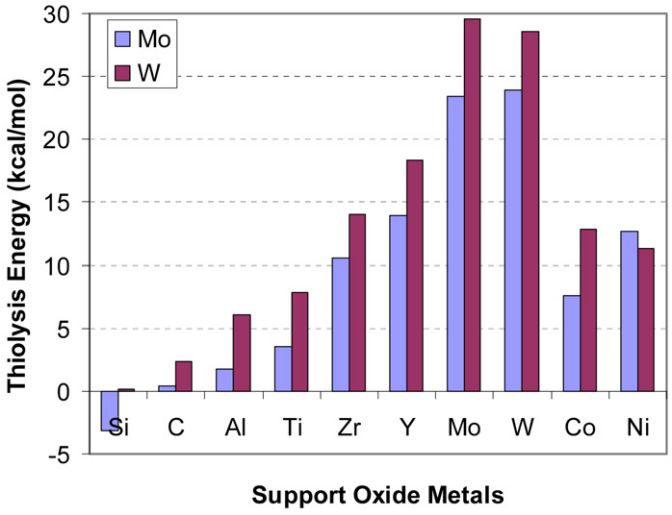

(a)

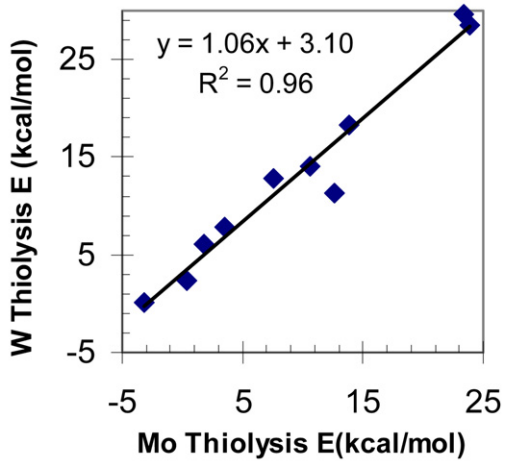

(b)

Fig. 7. Thiolysis energies of Mo and W linkages with support metals; (a) bar chart showing thiolysis energies for Mo and W; (b) linear correlation between Mo and W.

4. Conclusions

We have found that the thiolysis reaction energy for a simple model of the metal–support linkage explains several experimental observations. The expected increase in the transition-metal–sulfide dispersion follows the order of Si < C < Al < Ti < Zr < Y, which is in the agreement with the experimentally observed trends. For Si and Al, the quantitative values of the thiolysis energy explain some important observations such as Type-I → Type-II transformation on high temperature sulfidation of Mo/Al_2O_3 catalyst. We also find that trends in the thiolysis energy correlate well with the contribution of the Mo to the NBO involving the bridging oxygen atom to the support metals. It is encouraging that the relatively simple model used here is able to produce a descriptor that appears to have value for predicting catalyst behavior. Such descriptors will be the foundation of evolving efforts to achieve true catalyst design.

Acknowledgments

We would like to thank Dr. Stuart Soled from ExxonMobil Research and Engineering for providing experimental insights regarding various support types. Computational resources were obtained through supercomputing resources at Purdue University.

References

[1] G.M. Dhar, B.N. Srinivas, M.S. Rana, M. Kumar, S.K. Maity, Catal. Today 86 (2003) 45.
[2] S. Srinivasan, A.K. Datye, C.H.F. Peden, J. Catal. 137 (1992) 513.
[3] A.K. Datye, S. Srinivasan, L.F. Allard, C.H.F. Peden, J.R. Brenner, L.T. Thompson, J. Catal. 158 (1996) 205.
[4] K.C. Pratt, J.V. Sanders, V. Christov, J. Catal. 124 (1990) 416.
[5] S.K. Maity, M.S. Rana, B.N. Srinivas, S.K. Bej, G. Murali Dhar, T.S.R. Prasada Rao, J. Mol. Catal. A Chem. 153 (2000) 121.
[6] K.V.R. Chary, H. Ramakrishna, K.S. Rama Rao, G. Murali Dhar, P. Kanta Rao, Catal. Lett. 10 (1991) 27.
[7] K.S. Rawat, M.S. Rana, G. Murali Dhar, in: A. Galarneau, F. Fajula, F.D. Renzo, J. Vedrine (Eds.), Stud. Surf. Sci. Catal., Elsevier, 2001, p. 301.
[8] A. Wang, Y. Wang, T. Kabe, Y. Chen, A. Ishihara, W. Qian, J. Catal. 199 (2001) 19.
[9] K.M. Reddy, B. Wei, C. Song, Catal. Today 43 (1998) 261.
[10] C. Song, K.M. Reddy, Appl. Catal. A 176 (1999) 1.
[11] S.K. Maity, B.N. Srinivas, V.V.D.N. Prasad, A. Singh, G. Murali Dhar, T.S.R. Prasada Rao, in: T.S.R. Prasada Rao, G. Murali Dhar (Eds.), Stud. Surf. Sci. Catal., Elsevier, 1998, p. 579.
[12] J. Ramirez, L. Ruiz-Ramirez, L. Cedeno, V. Harle, M. Vrinat, M. Breysse, Appl. Catal. A 93 (1993) 163.
[13] W. Zhaobin, X. Qin, G. Xiexian, E.L. Sham, P. Grange, B. Delmon, Appl. Catal. 63 (1990) 305.
[14] W. Zhaobin, X. Qin, G. Xiexian, P. Grange, B. Delmon, Appl. Catal. 75 (1991) 179.
[15] K. Segawa, S. Satoh, G.F.F.a.P.G.B. Delmon, in: Stud. Surf. Sci. Catal., Elsevier, 1999, p. 129.
[16] S. Yoshinaka, K. Segawa, Catal. Today 45 (1998) 293.
[17] C. Pophal, F. Kameda, K. Hoshino, S. Yoshinaka, K. Segawa, Catal. Today 39 (1997) 21.
[18] R. Candia, O. Sorensen, J. Villadsen, N.Y. Topsøe, B.S. Clausen, H. Topsøe, Bull. Soc. Chim. Belg. 93 (1984) 763.
[19] N. Topsøe, J. Catal. 64 (1980) 235.
[20] J.A.R. van Veen, P. Hendriks, E. Romers, R.R. Andrea, J. Phys. Chem. 94 (1990) 5275.
[21] J.A.R. van Veen, P. Hendriks, R.R. Andrea, E. Romers, A.E. Wilson, J. Phys. Chem. 94 (1990) 5282.
[22] E.J.M. Hensen, P.J. Kooyman, Y. van der Meer, A.M. van der Kraan, V.H.J. de Beer, J.A.R. van Veen, R.A. van Santen, J. Catal. 199 (2001) 224.
[23] B. Hinnemann, J.K. Nørskov, H. Topsøe, J. Phys. Chem. B 109 (2005) 2245.
[24] Y. Sakashita, T. Yoneda, J. Catal. 185 (1999) 487.
[25] C. Arrouvel, M. Breysse, H. Toulhoat, P. Raybaud, J. Catal. 232 (2005) 161.
[26] A.M. de Jong, H.J. Borg, L.J. van IJzendoorn, V. Soudant, V.H.J. de Beer, J.A.R. van Veen, J.W. Niemantsverdriet, J. Phys. Chem. 97 (1993) 6477.
[27] G. Kishan, L. Coulier, V.H.J. de Beer, J.A.R. van Veen, J.W. Niemantsverdriet, J. Catal. 196 (2000) 180.
[28] G. Kishan, L. Coulier, J.A.R. van Veen, J.W. Niemantsverdriet, J. Catal. 200 (2001) 194.
[29] F. Besenbacher, M. Brorson, B.S. Clausen, S. Helveg, B. Hinnemann, J. Kibsgaard, J.V. Lauritsen, P.G. Moses, J.K. Nørskov, H. Topsøe, Catal. Today 130 (2008) 86.
[30] P. Raybaud, Appl. Catal. A 322 (2007) 76.
[31] C. Thomazeau, C. Geantet, M. Lacroix, M. Danot, V. Harle, P. Raybaud, Appl. Catal. A 322 (2007) 92.
[32] C. Arrouvel, M. Digne, M. Breysse, H. Toulhoat, P. Raybaud, J. Catal. 222 (2004) 152.
[33] C. Arrouvel, H. Toulhoat, M. Breysse, P. Raybaud, J. Catal. 226 (2004) 260.
[34] D. Costa, C. Arrouvel, M. Breysse, H. Toulhoat, P. Raybaud, J. Catal. 246 (2007) 325.
[35] N.Y. Topsøe, H. Topsøe, J. Catal. 139 (1993) 641.
[36] R.G. Leliveld, A.J. van Dillen, J.W. Geus, D.C. Koningsberger, J. Catal. 165 (1997) 184.
[37] A.D. Becke, J. Chem. Phys. 98 (1993) 5648.
[38] C. Lee, W. Yang, R.G. Parr, Phys. Rev. B Condens. Mater 37 (1988) 785.
[39] M.M. Francl, W.J. Pietro, W.J. Hehre, J.S. Binkley, M.S. Gordon, D.J. DeFrees, J.A. Pople, J. Chem. Phys. 77 (1982) 3654.
[40] P.J. Hay, W.R. Wadt, J. Chem. Phys. 82 (1985) 270.
[41] W.R. Wadt, P.J. Hay, J. Chem. Phys. 82 (1985) 284.
[42] P.J. Hay, W.R. Wadt, J. Chem. Phys. 82 (1985) 299.
[43] Gaussian 03, Revision C.02, M.J. Frisch, G.W. Trucks, H.B. Schlegel, G.E. Scuseria, M.A. Robb, J.R. Cheeseman, J. Montgomery, J.A.T. Vreven, K.N. Kudin, J.C. Burant, J.M. Millam, S.S. Iyengar, J. Tomasi, V. Barone, B. Mennucci, M. Cossi, G. Scalmani, N. Rega, G.A. Petersson, H. Nakatsuji, M. Hada, M. Ehara, K. Toyota, R. Fukuda, J. Hasegawa, M. Ishida, T. Nakajima, Y. Honda, O. Kitao, H. Nakai, M. Klene, X. Li, J.E. Knox, H.P. Hratchian, J.B. Cross, C. Adamo, J. Jaramillo, R. Gomperts, R.E. Stratmann, O. Yazyev, A.J. Austin, R. Cammi, C. Pomelli, J.W. Ochterski, P.Y. Ayala, K. Morokuma, G.A. Voth, P. Salvador, J.J. Dannenberg, V.G. Zakrzewski, S. Dapprich, A.D. Daniels, M.C. Strain, O. Farkas, D.K. Malick, A.D. Rabuck, K. Raghavachari, J.B. Foresman, J.V. Ortiz, Q. Cui, A.G. Baboul, S. Clifford, J. Cioslowski, B.B. Stefanov, G. Liu, A. Liashenko,

P. Piskorz, I. Komaromi, R.L. Martin, D.J. Fox, T. Keith, M.A. Al-Laham, C.Y. Peng, A. Nanayakkara, M. Challacombe, P.M.W. Gill, B. Johnson, W. Chen, M.W. Wong, C. Gonzalez, J.A. Pople, Gaussian, Inc., Wallingford, CT, 2004.
[44] J.P. Foster, F. Weinhold, J. Am. Chem. Soc. 102 (1980) 7211.
[45] A.E. Reed, F. Weinhold, J. Chem. Phys. 78 (1983) 4066.
[46] A.E. Reed, L.A. Curtiss, F. Weinhold, Chem. Rev. 88 (1988) 899.
[47] L. Kaluza, D. Gulkova, Z. Vit, M. Zdrazil, Appl. Catal. A 324 (2007) 30.
[48] S.L. Soled, S. Miseo, J.E. Baumgartner, C.E. Kliewer, J.T. Elks, US Patent US 2007/0082811 A1 (2007), to ExxonMobil Research and Engineering Company.
[49] R. Cattaneo, T. Weber, T. Shido, R. Prins, J. Catal. 191 (2000) 225.
[50] L. Coulier, V.H.J. de Beer, J.A.R. van Veen, J.W. Niemantsverdriet, J. Catal. 197 (2001) 26.
[51] L. Medici, R. Prins, J. Catal. 163 (1996) 38.
[52] R. Cattaneo, T. Shido, R. Prins, J. Catal. 185 (1999) 199.
[53] M. Vrinat, M. Lacroix, M. Breysse, R. Frety, Bull. Soc. Chim. Belg. 93 (1984) 697.
[54] H. Toulhoat, P. Raybaud, S. Kasztelan, G. Kresse, J. Hafner, Catal. Today 50 (1999) 629.
[55] R. Thomas, E.M. van Oers, V.H.J. de Beer, J. Medema, J.A. Moulijn, J. Catal. 76 (1982) 241.
[56] P.J. Mangnus, B. Scheffer, J.A. Moulijn, Abstr. Pap. Am. Chem. Soc. 193 (1987) 36.